# Fully Coherent UAV-Based Near-Field Measurement and Transformation of the S67-15 m Ground Station Antenna at the German Space Operations Center in Weilheim

Stefan Punzet*, Fabian T. Faul*, Thomas Mittereder*, Christian Oettl†, Matthias Ganser†, Martin Häusler†, Thomas F. Eibert*

*Chair of High-Frequency Engineering, Department of Electrical and Computer Engineering, Technical University of Munich, 80290, Munich, Germany, e-mail: {stefan.punzet; eibert}@tum.de

†DLR Deutsches Zentrum für Luft- und Raumfahrt e. V., 82362, Weilheim, Germany

***Abstract*—Fully coherent unmanned aerial vehicle (UAV)-based near-field measurements of the S67 parabolic ground station antenna in Weilheim, Germany at 2.063 92 GHz are presented. The utilized measurement setup involves a vector network analyzer (VNA), radio frequency optical fiber connections, a laser tracking device (LT), and a specially designed light-weight dual-polarized Vivaldi antenna. The measurement data has been collected on a quasi-planar measurement surface in front of the reflector and the far-field patterns are obtained by field transformation from the irregular near-field data. Despite the complexity of this outdoor measurement setup with full exposure to varying weather conditions and the influence of the UAV on the near-field probe antenna, the far-field results show remarkable agreement with satellite based far-field measurement data.**

***Index Terms*—antenna, near field, fully coherent measurement, unmanned aerial vehicle.**

## I. Introduction

Traditionally, antenna characteristics, such as radiation pattern, directivity and gain are measured by placing the antenna under test (AUT) inside an anechoic chamber and by sampling the electromagnetic (EM) field utilizing highly sensitive radio frequency (RF) measurement devices along with highly precise positioning systems [1], [2]. This conventional approach can not be applied for stationary physically large antennas or multi-antenna systems. However, the exact antenna far-field characteristics of such antennas and multi-antenna systems are of particular interest for operational and safety reasons.

Physically large ground station antennas are commonly used in long distance communication links, e.g., for satellite communication. Therefore, such antennas must exhibit high gain and directivity to overcome the high pathloss between transmitter (TX) and receiver (RX). It is possible to measure the antenna far-field characteristics of such antennas if there is a direct line of sight to a satellite or a second base station antenna [3]–[5]. However, reflections, e.g., off the ground, as well as atmospheric and man-made interference along the RF path degrade the measurement results. Additionally, not all satellites or ground station antennas support multiple polarizations. Hence, a dual-polarized AUT can not be fully characterized. Furthermore, not only the AUT but also the satellite or second ground station antenna is blocked during the measurement and can, therefore, not be used for other missions. Given the tight operational schedule of satellites and ground station antennas, this measurement procedure can rarely be employed.

Another possibility to obtain the antenna far-field characteristic is to sample the antenna near-field in situ and then perform a near-field-to-far-field transformation (NFFFT). Performing in-situ measurements of physically large antennas requires novel and portable measurement solutions. Due to decreasing cost and increasing availability, unmanned aerial vehicles (UAVs) are used more commonly in a large variety of applications, also impacting antenna measurements [6]–[17]. UAV-based antenna measurements require specialized probe antennas and RF measurement equipment due to size and weight constraints of the specific UAV. Furthermore, the UAV is exposed to weather conditions. In particular, sampling of the EM near field on a regular grid can not be guaranteed. This is especially challenging for the NFFFT requiring advanced transformation algorithms, such as the fast irregular antenna field transformation algorithm (FIAFTA) [2], [18]–[20].

With this in mind, most UAV-based antenna measurements are focused on far-field measurements [6], [9], [13] or on specialized procedures such as phaseless measurements and transformations [8], [14], [21], [22]. A fully coherent near-field measurement and transformation for a rather small test antenna was presented in [16]. In the current work, we follow a similar strategy to perform fully coherent near-field measurements and transformations for the S67-15 m ground station antenna at the German space operations center (GSOC) in Weilheim. The measurements have been performed in S-band for a frequency of $f_{\mathrm{meas}} = 2.063\,92\,\mathrm{GHz}$, where the AUT showed best input matching and maximum distance to nearby mobile communication bands (Long-Term Evolution (LTE): $2.11\,\mathrm{GHz} - 2.20\,\mathrm{GHz}$ [23, p. 45] and LTE+Universal Mobile Telecommunications System (UMTS): $1.92\,\mathrm{GHz} - 2.01\,\mathrm{GHz}$ [24, p. 21]) is maintained. A laser

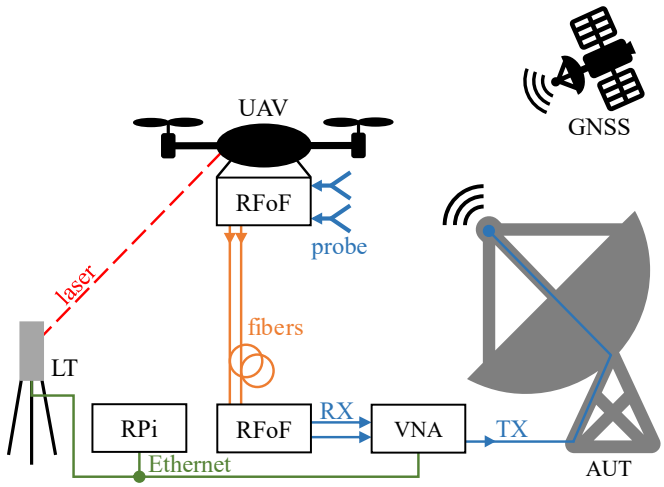


Fig. 1. Schematic representation of the measurement setup comprising the UAV with attached dual-polarized probe antenna, positioning system (GNSS and LT), RF measurement equipment and central controlling unit (RPi).

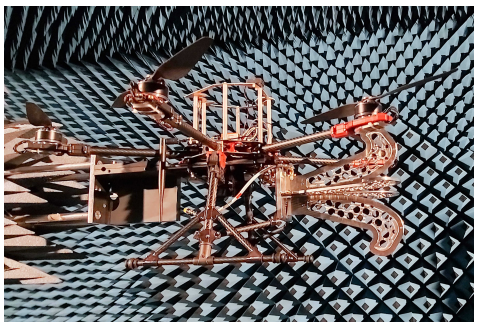

Fig. 2. Hexa-copter UAV with attached dual-polarized probe antenna mounted in the anechoic antenna measurement chamber at the Technical University of Munich (TUM).

tracker (LT) [25] was used to accurately obtain the measurement sample locations [26], [27], whereas the flight control was based on a real-time kinematic (RTK) global navigation satellite system (GNSS). The fully coherent measurement setup consisted of a vector network analyzer (VNA) together with optical fiber connections for a specialized dual-polarized Vivaldi antenna [28].

Section II of this paper describes the measurement setup in detail and in Section III the near-field measurement results and the transformed far-field patterns are presented and discussed, before some conclusions are drawn in Section IV.

## II. Measurement Setup

Fig. 1 shows the utilized measurement setup comprising the UAV with attached probe antenna, the positioning system, RF measurement equipment and controlling unit. The individual components of the setup are described in more detail in the following.

Fig. 2 shows the utilized Hexa-copter UAV with mounted probe antenna. The probe antenna is dual polarized, made of aluminum and optimized for UAV-based applications [28].

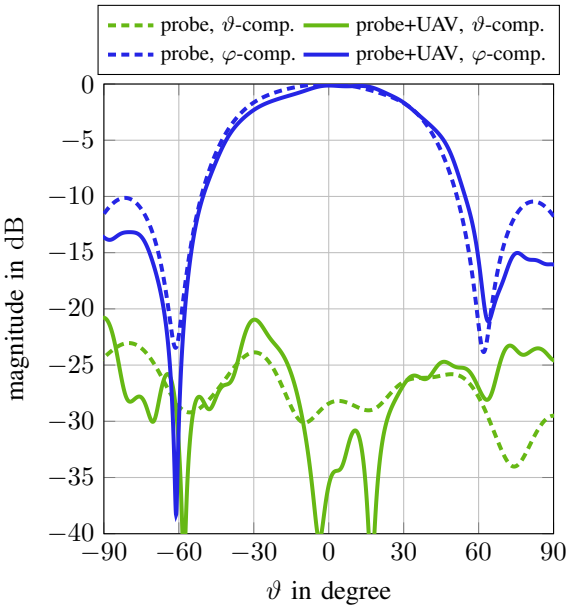


(a) Horizontal polarization of the probe in the cut at $\varphi = 0°$.

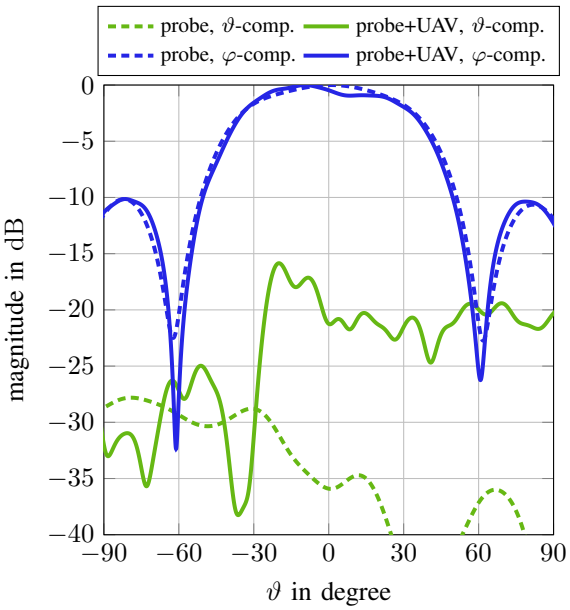


(b) Vertical polarization of the probe in the cut at $\varphi = 90°$.

Fig. 3. Exemplary cuts of the far-field patterns of the two polarizations of the probe antenna without UAV (probe) and with mounted UAV (probe+UAV) measured in the anechoic antenna measurement chamber at the Technical University of Munich (TUM), see Fig. 2.

The antenna mounting mechanism is custom fabricated and designed. The overall design is weight-optimized to approximately 400 g while maintaining sufficient mechanical rigidity for consistent alignment of the probe antenna to the UAV during measurement flights.

Fig. 3 shows the measured probe antenna pattern without UAV (probe) and with attached UAV (probe+UAV) for both horizontal (Fig. 3(a)) and vertical (Fig. 3(b)) polarization to account for influences of the UAV on the probe antenna pat-


Fig. 4. Measurement setup with LT and flying UAV to sample the near field of the AUT S67 at the GSOC in Weilheim, Germany. The AUT follows the Cassegrain principle with a main reflector of $\varnothing\,15\,\mathrm{m}$ and is operating in the S-band ($2\,\mathrm{GHz}-4\,\mathrm{GHz}$).

tern. The presence of the UAV significantly changes the probe antenna characteristics. Thus, the FIAFTA built-in probe-correction routines account for the actual probe characteristics to still achieve correct far-field results.

Towards the preparation of the UAV-based measurements, a measurement surface is defined by the user and divided into planar or elliptical scan paths, which are uploaded to the UAV flight controller (FC). Next, the UAV autonomously flies along the stored flight paths, guided by GNSS. We use an RTK GNSS setup with an own on-site RTK base station to achieve a position accuracy of the UAV of approximately $10\,\mathrm{cm}$. This is precise enough for safe and reliable operation of the UAV even in close proximity to the AUT. However, this position accuracy is by far not good enough to determine the position of the field sample locations and to achieve proper NFFFT results. The field transformation is highly dependent on the exact knowledge of the probe position and orientation. As a rule of thumb, a position accuracy better than $\lambda_0/50$, which corresponds to approximately $3.00\,\mathrm{mm}$ at $f_0 = 2\,\mathrm{GHz}$, should be achieved. Therefore, a 3-dimensional (3D) LT measures the exact 3D position of the UAV within tens of micrometers during the measurement flight. Furthermore, redundant inertial measurement units (IMUs) built into the FC determine the UAV orientation and hence the orientation of the probe antenna within fractions of a degree. Finally, we fuse all sensor data of IMUs, GNSS and LT in post processing to obtain most accurate position and orientation data of the probe antenna.

A 4-port VNA feeds the continuous wave (CW) signal to the AUT and coherently samples the EM near field for both, vertical and horizontal polarization of the probe antenna. The VNA remains on the ground since it is too large and heavy to mount it to the UAV. Hence, the received RF signals of the

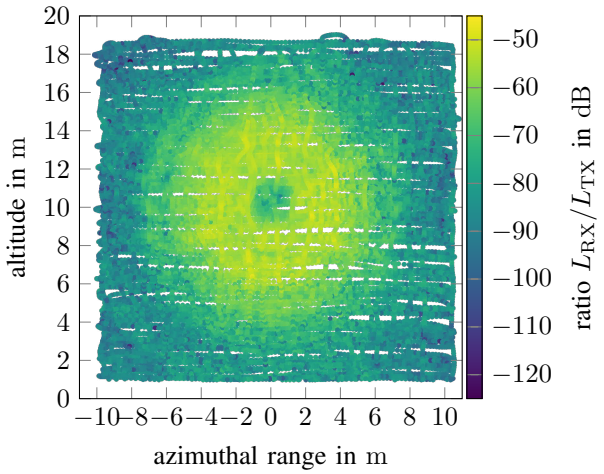


(a) Measured near-field magnitude – horizontal polarization.

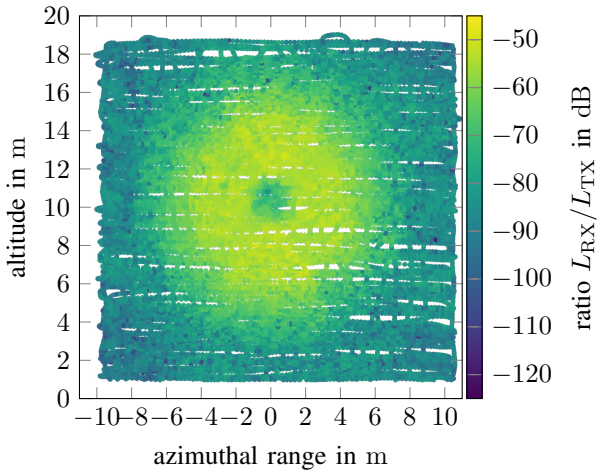


(b) Measured near-field magnitude – vertical polarization.

Fig. 5. Magnitude of the sampled near-field for (a) horizontal and (b) vertical polarization of the probe antenna. The near field is irregularly sampled at 23 742 points on a $20\,\mathrm{m} \times 18\,\mathrm{m}$ quasi-planar surface in approximately $5\,\mathrm{m}$ distance to the AUT subreflector, see Fig. 4.

dual-polarized probe antenna are transmitted to the VNA on the ground via an optical fiber link. A separate RF over fiber (RFoF) converter is used for each polarization.

A Raspberry-Pi (RPi) single-board computer acts as central controlling unit. It simultaneously triggers the LT and VNA for coherent data acquisition of position and EM field data and gathers all data of the measurement equipment.

Fig. 4 shows the utilized measurement setup with LT and flying UAV to sample the near field of the AUT S67 at the GSOC in Weilheim, Germany. The antenna is working in the S-band ($2\,\mathrm{GHz}-4\,\mathrm{GHz}$) and follows the Cassegrain principle with a main reflector of $15\,\mathrm{m}$ in diameter. During the measurement campaign, the AUT was set to an elevation of $6°$ above the horizon and transmitted a left-hand circular polarized (LHCP) CW signal at the frequency $f_{\mathrm{meas}} = 2.063\,92\,\mathrm{GHz}$ with a power of $L = 30\,\mathrm{dBm}$. For operational safety, a distance of approx-

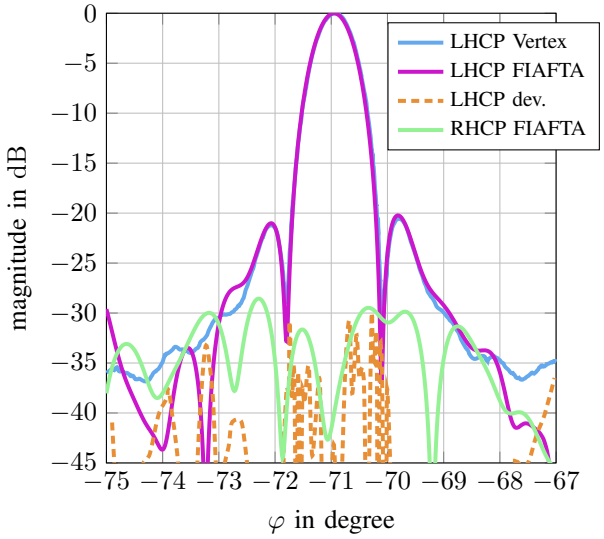


(a) AUT far-field pattern. Horizontal cut at $\vartheta = 83.65°$.

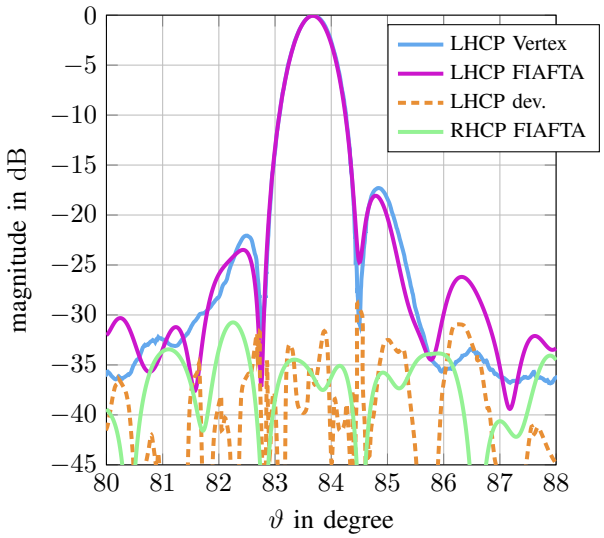


(b) AUT far-field pattern. Vertical cut at $\varphi = 289.10°$.

Fig. 6. Transformed AUT far-field patterns (a) horizontal cut and (b) vertical cut in comparison to far-field data from [29]. The sampled near-field data shown in Fig. 5 was first transformed using FIAFTA and then converted to a frequency of $f_{\mathrm{Vertex}} = 2.232\,765\,\mathrm{GHz}$, again using FIAFTA, for comparison with the far-field data in [29].

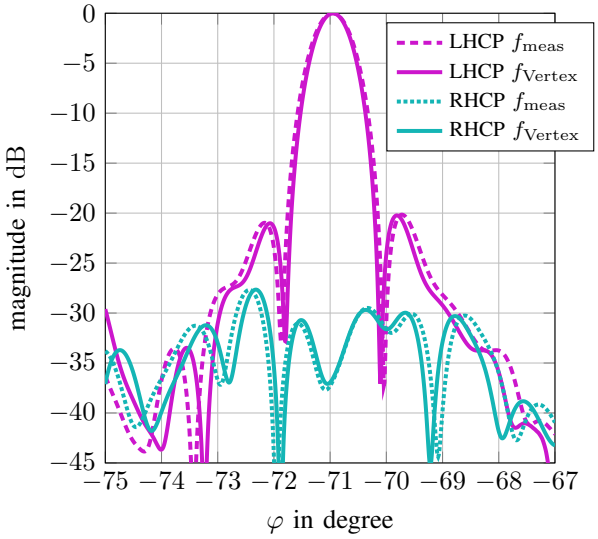


(a) FIAFTA far-field results. Horizontal cut at $\vartheta = 83.65°$.

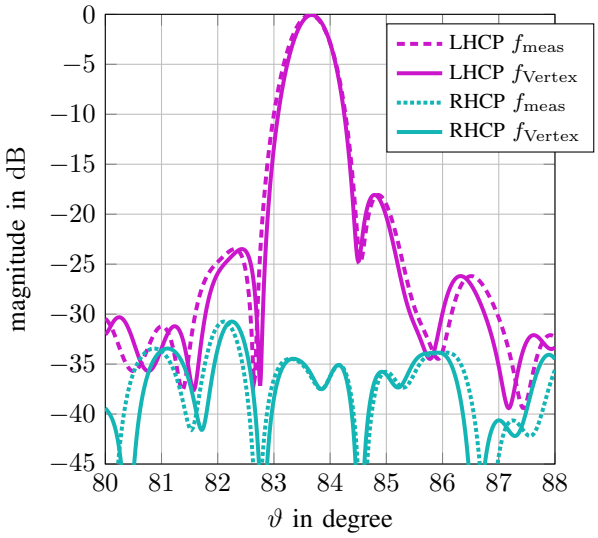


(b) FIAFTA far-field results. Vertical cut at $\varphi = 289.10°$.

Fig. 7. Comparison of FIAFTA transformed AUT far-field patterns (a) horizontal cut and (b) vertical cut for the measurement frequency $f_{\mathrm{meas}} = 2.063\,92\,\mathrm{GHz}$ and the frequency $f_{\mathrm{Vertex}} = 2.232\,765\,\mathrm{GHz}$ as used in [29]. The data at $f_{\mathrm{Vertex}}$ was computed from the measured data by using FIAFTA. As expected, the width of the main beam slightly decreases with increasing frequency.

imately $5\,\mathrm{m}$ is kept between UAV and AUT subreflector.

## III. Measurement Results

Fig. 5 shows the magnitude of the near field, sampled 23 742 times on a $20\,\mathrm{m} \times 18\,\mathrm{m}$ quasi-planar surface at a distance of approximately $5\,\mathrm{m}$ to the AUT subreflector (see Fig. 4) for horizontal (Fig. 5(a)) and vertical (Fig. 5(b)) polarization of the probe antenna. The irregular sampling of the near field shown in Fig. 5 is caused by the flight dynamics of the UAV together with unpredictably changing weather conditions during the measurement flights. The shading effect of the subreflector in the AUT center, as well as the field tapering of the antenna towards its outer edges are clearly visible.

Fig. 6 shows the transformed AUT far-field patterns for horizontal (Fig. 6(a)) and vertical (Fig. 6(b)) cuts. The sampled near-field data of Fig. 5 was first transformed using FIAFTA and then converted to a frequency of $f_{\mathrm{Vertex}} = 2.232\,765\,\mathrm{GHz}$ for comparison with the far-field data in [29]. The measurement in [29] was carried out utilizing the geostationary satellite Xtar-EUR (29.0°E) as TX for LHCP only. The UAV-based measurements could not be performed at the frequency $f_{\mathrm{Vertex}}$ due to operational restrictions. Our transformed far-field data

and the data in [29] show remarkable agreement, especially in main lobe direction. The shown deviation was computed as normalized linear magnitude difference.

Fig. 7 shows the transformed AUT far-field patterns for the actual measurement frequency $f_{\mathrm{meas}} = 2.063\,92\,\mathrm{GHz}$ compared to the re-computed far-field patterns for $f_{\mathrm{Vertex}} = 2.232\,765\,\mathrm{GHz}$ (as used in [29]). Since the frequency merely increases by $\Delta f = f_{\mathrm{Vertex}} - f_{\mathrm{meas}} = 168.845\,\mathrm{MHz}$ the antenna patterns do not change drastically. However, as expected, the antenna main beam width slightly decreases with increasing frequency.

## IV. Conclusion

Fully coherent UAV-based near-field measurements were performed for a $\varnothing\,15\,\mathrm{m}$ ground station antenna. The near-field was sampled at $23\,742$ points on an irregular grid on a $20\,\mathrm{m} \times 18\,\mathrm{m}$ quasi-planar surface in approximately $5\,\mathrm{m}$ distance to the AUT subreflector. The measured near-field data was transformed to far-field antenna patterns using FIAFTA. The obtained far-field patterns show remarkable agreement with the far-field data in [29], which was obtained from satellite based measurements.

## Acknowledgment

This work was supported in part by the German Federal Ministry for Economic Affairs and Energy (BMWi) under Grant 50RK1923.

## References

[1] C. Parini, S. F. Gregson, J. McCormick, D. J. van Rensburg, and T. Eibert, *Theory and Practice of Modern Antenna Range Measurements*, 2nd ed. Institution of Engineering and Technology - IET, 2020, vol. 1.

[2] ——, *Theory and Practice of Modern Antenna Range Measurements*, 2nd ed. Institution of Engineering and Technology - IET, 2020, vol. 2.

[3] E. Ekleman and S. Frimel, "On-site earth station antenna verification," in *IEEE Antennas and Propagation Society International Symposium*, vol. 4, 1992, pp. 2060–2063.

[4] K. Ueno, "A study on a satellite antenna pointing measurement system," in *IEEE Antennas and Propagation Society International Symposium and URSI National Radio Science Meeting*, vol. 1, 1994, pp. 282–285 vol.1.

[5] G. Hua, Y. Ma, and Jirigele, "Studies on satellite antenna gain measurement system based on comparison method," in *IEEE 6th International Symposium on Microwave, Antenna, Propagation, and EMC Technologies (MAPE)*, 2015, pp. 242–244.

[6] F. Paonessa *et al.*, "UAV-based pattern measurement of the SKALA," in *IEEE International Symposium on Antennas and Propagation & USNC/URSI National Radio Science Meeting*, 2015, pp. 1372–1373.

[7] T. Fritzel, R. Strauß, H.-J. Steiner, C. Eisner, and T. Eibert, "Introduction into an UAV-based near-field system for in-situ and large-scale antenna measurements (invited paper)," in *IEEE Conference on Antenna Measurements Applications (CAMA)*, 2016, pp. 1–3.

[8] M. García-Fernández *et al.*, "Antenna diagnostics and characterization using unmanned aerial vehicles," *IEEE Access*, vol. 5, pp. 23 563–23 575, 2017.

[9] A. N. Cadavid, J. Aristizabal, and M. D. P. Alhucema, "Antenna pattern verification for digital TV broadcast systems in andean countries based on UAV's," in *IEEE-APS Topical Conference on Antennas and Propagation in Wireless Communications (APWC)*, 2018, pp. 858–861.

[10] M. García Fernández, Y. Álvarez López, and F. Las-Heras, "Dual-probe near-field phaseless antenna measurement system on board a UAV," *Sensors*, vol. 19, no. 21, 2019. [Online]. Available: https://www.mdpi.com/1424-8220/19/21/4663

[11] ——, "Unmanned aerial system for antenna measurement and diagnosis: evaluation and testing," *IET Microwaves, Antennas & Propagation*, vol. 13, no. 13, pp. 2224–2231, 2019.

[12] L. Ciorba *et al.*, "Near-field phase reconstruction for UAV-based antenna measurements," in *13th European Conference on Antennas and Propagation (EuCAP)*, 2019, pp. 1–4.

[13] A. Y. Umeyama, J. L. Salazar-Cerreno, and C. J. Fulton, "UAV-based far-field antenna pattern measurement method for polarimetric weather radars: Simulation and error analysis," *IEEE Access*, vol. 8, pp. 191 124–191 137, 2020.

[14] Y. Álvarez López, M. García-Fernández, and F. Las-Heras, "A portable cost-effective amplitude and phase antenna measurement system," *IEEE Transactions on Instrumentation and Measurement*, vol. 69, no. 9, pp. 7240–7251, 2020.

[15] F. Paonessa *et al.*, "Design and verification of a Q-band test source for UAV-based radiation pattern measurements," *IEEE Transactions on Instrumentation and Measurement*, vol. 69, no. 12, pp. 9366–9370, 2020.

[16] F. T. Faul and T. F. Eibert, "Setup and error analysis of a fully coherent UAV-based near-field measurement system," in *15th European Conference on Antennas and Propagation (EuCAP)*, 2021, pp. 1–4.

[17] H.-J. Steiner, T. Fritzel, and R. Strauß, "Aspects of near-field antenna measurement technology when using UAV's," in *15th European Conference on Antennas and Propagation (EuCAP)*, 2021, pp. 1–5.

[18] T. F. Eibert and C. H. Schmidt, "Multilevel fast multipole accelerated inverse equivalent current method employing Rao–Wilton–Glisson discretization of electric and magnetic surface currents," *IEEE Transactions on Antennas and Propagation*, vol. 57, no. 4, pp. 1178–1185, 2009.

[19] T. F. Eibert, E. Kiliç, C. Lopez, R. A. M. Mauermayer, O. Neitz, and G. Schnattinger, "Electromagnetic field transformations for measurements and simulations (invited paper)," *Progress In Electromagnetics Research*, vol. 151, pp. 127–150, 5 2015.

[20] J. Kornprobst, R. A. M. Mauermayer, O. Neitz, J. Knapp, and T. F. Eibert, "On the solution of inverse equivalent surface-source problems," *Progress In Electromagnetics Research*, vol. 165, pp. 47–65, 8 2019.

[21] M. García-Fernández, Y. Álvarez López, and F. Las-Heras Andrés, "Antenna measurement and diagnostics processing techniques using unmanned aerial vehicles," in *13th European Conference on Antennas and Propagation (EuCAP)*, 2019, pp. 1–5.

[22] ——, "Advances in antenna measurement and characterization using unmanned aerial vehicles," in *13th European Conference on Antennas and Propagation (EuCAP)*, 2019, pp. 1–5.

[23] *LTE; Evolved Universal Terrestrial Radio Access (E-UTRA); User Equipment (UE) radio transmission and reception*, European Telecommunications Standards Institute (ETSI) technical specification 3GPP TS 36.101, Rev. 16.11.0 Release 16, 11 2021. [Online]. Available: https://www.etsi.org/deliver/etsi_ts/136100_136199/136101/16.11.00_60/ts_136101v161100p.pdf

[24] *Universal Mobile Telecommunications System (UMTS); User Equipment (UE) radio transmission and reception (FDD)*, European Telecommunications Standards Institute (ETSI) technical specification 3GPP TS 25.101, Rev. 16.1.0 Release 16, 11 2020. [Online]. Available: https://www.etsi.org/deliver/etsi_ts/125100_125199/125101/16.01.00_60/ts_125101v160100p.pdf

[25] FARO. (2021, 7) FARO® vantage laser trackers. FARO Technologies, Inc. SFDC_04MKT_488 Rev. 07/21/2021. [Online]. Available: https://media.faro.com/-/media/Project/FARO/FARO/FARO/Resources/FARO-Vantage-Laser-Trackers/TechSheet_Vantage_DEU.pdf?rev=-1

[26] T. Fritzel, H.-J. Steiner, and R. Strauß, "Laser tracker metrology for UAV-based antenna measurements," in *IEEE Conference on Antenna Measurements Applications (CAMA)*, 2018, pp. 1–3.

[27] P. Henkel, A. Sperl, U. Mittmann, T. Fritzel, R. Strauss, and H. Steiner, "Precise 6D RTK positioning system for UAV-based near-field antenna measurements," in *14th European Conference on Antennas and Propagation (EuCAP)*, 2020, pp. 1–5.

[28] A. Azhar and T. F. Eibert, "A dual-polarized tapered slot antenna for UAV-based collection of locally coherent field data," in *15th European Conference on Antennas and Propagation (EuCAP)*, 2021, pp. 1–4.

[29] Vertex Antennentechnik GmbH, "S67 DLR Weilheim Modernisierungskonzept: Gutachten für die Erstellung eines Renovierungskonzeptes für S-Band Systeme am DLR Standort Weilheim," unpublished, Vertex Antennentechnik GmbH, Duisburg, Germany, Tech. Rep., 4 2021.